FOCUSED ISSUE FEATURE

Artificial Dielectrics

Rajind Mendis and Daniel M. Mittleman

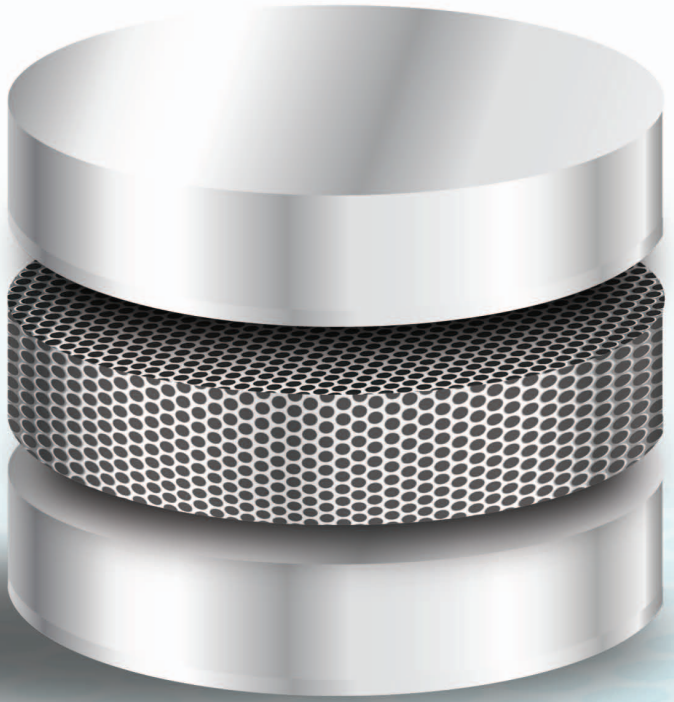

Consider an electromagnetic wave propagating in the empty space between two parallel metal plates. This situation is often the first example of guided waves encountered by undergraduate students since the solutions (the guided modes) are analytic and easily obtained. And yet, this seemingly simple configuration can give rise to a number of interesting and even counterintuitive phenomena. For the set of modes with the electric field pointing parallel to the surfaces of the two metal plates, the region between the plates, though simply empty space, mimics the properties of a dielectric medium with a wave velocity v_p different from c, that of waves in vacuum. The waveguide therefore can be described as an artificial dielectric [1] with an effective refractive index $n = c/v_p$ different from unity. In contrast to naturally occurring dielectrics for which $n > 1$, n can have a value less than unity. These waveguide-based artificial dielectrics were first introduced in a small body of work by the microwave community about half a century ago [2]–[5]. As discussed here [6]–[10], the wavelength scaling that results

Rajind Mendis (rajind@rice.edu) and Daniel M. Mittleman (daniel@rice.edu) are with the Department of Electrical and Computer Engineering, Rice University, Houston, Texas 77005, United States.

Digital Object Identifier 10.1109/MMM.2014.2355696
Date of publication: 12 November 2014

when moving from the microwave region to the terahertz (THz) region results in more practical structural dimensions. This gives new life to these artificial dielectrics for a variety of novel and exotic applications in THz science and technology.

Figure 1 illustrates one implementation (a lens-antenna) of some of the historical work [2]. These early devices consisted of a stack of metal plates, with each plate shaped into a unique geometry. They behaved as an array of parallel-plate waveguides (PPWGs) operating in tandem. In very general terms, these devices function (or affect refraction) very similarly to a naturally occurring dielectric medium, i.e., by imparting a change in the phase velocity of electromagnetic waves. Since the overall device consists of a stacked array of waveguides, we can understand the principle of operation by looking at a single PPWG: a unit cell. When the electric field of the input wave is polarized parallel to the plates, only the transverse-electric (TE) modes are excited in a PPWG. Furthermore, it is possible to excite only (or primarily) the lowest-order TE mode (the TE_1 mode) by matching the input beam size to the plate separation b.

As shown in Figure 2(a), the phase velocity v_p of the TE_1 mode has a characteristic frequency dependence; it increases from the free-space value c to infinity as the frequency approaches the cutoff frequency f_c. Using the well-known expression for v_p [11], we can derive an effective refractive index n, given by

$$n = c/v_p = \sqrt{1-(f_c/f)^2}, \tag{1}$$

where $f_c = c/(2b)$. This function is plotted in Figure 2(b) for two different values of the plate separation, showing that n varies from a value close to unity at high frequencies to zero as the frequency reaches cutoff. Therefore, a wave propagating in the TE_1 mode inside the PPWG experiences a medium with a refractive index n varying between zero and unity.

Using only a single PPWG, i.e., a single unit cell, would limit the functionality of these components to only two dimensions. To extend the functionality to the third dimension (and be able to handle large cross-sectional beam sizes), one can construct a stacked set of thin metal plates (as in Figure 1). However, even in this case, one does not achieve true three-dimensional (3-D) behavior since there cannot be any propagation in the direction perpendicular to the plates.

Equation (1) also reveals that the effective refractive index n depends on both the operating frequency and the plate separation. This implies that n can be tuned between zero and unity, either by varying the frequency for a given plate separation or by varying the plate separation for a given frequency. In the former case, at a given operating frequency, n would be uniform throughout, resulting in a *homogeneous* medium. In the latter case, n would vary spatially, resulting in an *inhomogeneous* medium. In fact, using the latter approach, one may create a desired refractive index profile (in two dimensions) simply by choosing an appropriate plate separation. This approach is effective as long as the change in the plate

To extend the functionality to the third dimension (and be able to handle large cross-sectional beam sizes), one can construct a stacked set of thin metal plates (as in Figure 1).

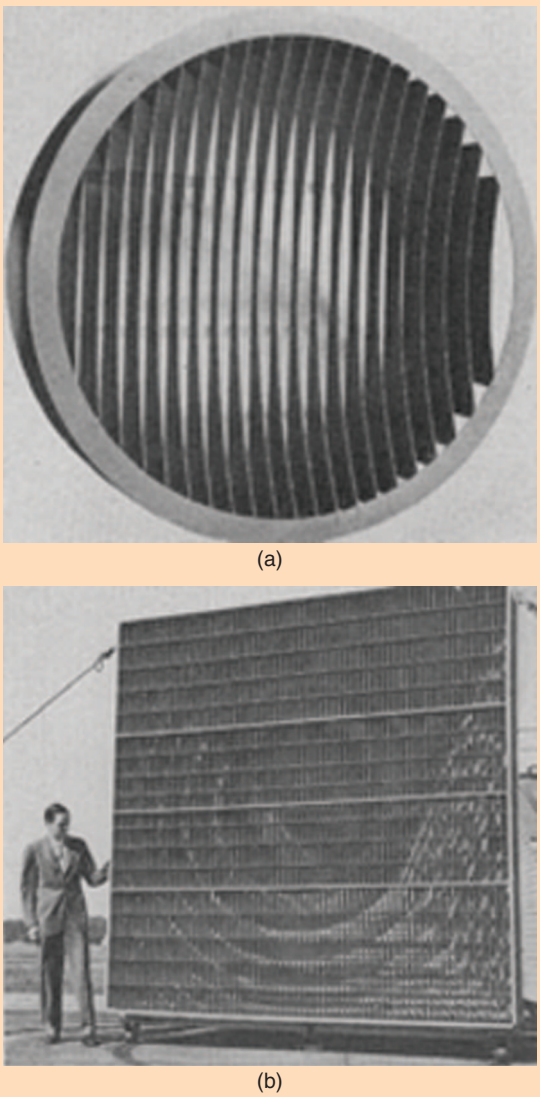

Figure 1. *Metal lens antennas using waveguide-based artificial dielectrics. (a) A plano-concave geometry that operates as a convergent lens. The aperture diameter is 14 wavelengths, and the focal length is 23 wavelengths. (b) A repeater antenna operating at 4 GHz. Note the structural size of the device compared to a human. (From [2].)*

separation is adiabatic with respect to the wavelength so that the single-mode nature of the input wave is preserved. In this case, even though the propagation would be governed by the characteristics of the TE_1 mode, the plates would no longer be precisely parallel to each other.

In the following sections, we describe some examples of the phenomena that can result from the use of these artificial dielectric structures and a few functional components that may be valuable in THz applications.

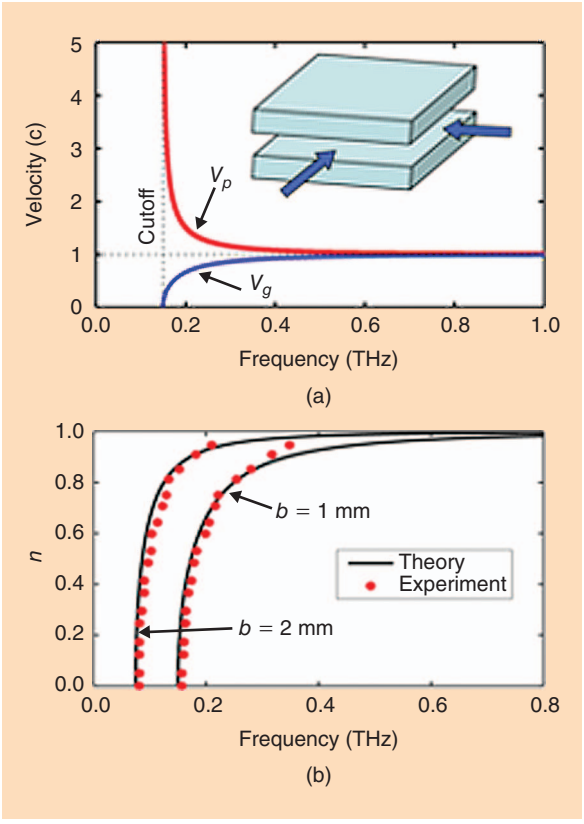

Figure 2. *(a) The phase and group velocity of the TE_1 mode with respect to the free-space value c, for a PPWG with $b = 1$ mm. The PPWG shown in the inset can operate only in two dimensions as indicated by the two arrows. (b) The effective refractive index for $b = 1$ mm and 2 mm, where $f_c = 0.15$ THz and 0.075 THz, respectively. (From [6].)*

Refraction

To demonstrate the refractive behavior of this artificial dielectric medium, one can perform an experiment using a 45° PPWG prism, fabricated using triangular aluminum plates [6]. A schematic and the device geometry are shown in Figure 3(a) and (b), respectively. As shown, a THz beam is coupled into the prism at normal incidence with the electric field polarized parallel to the plate surfaces. The beam consists of a train of broadband THz pulses with a spectral content that varies from about 0.05 THz to about 1 THz. The beam propagates via the TE_1 mode through the prism and encounters the exit face at an angle of 45°. At this face, if the artificial dielectric behaves as predicted, the wave should experience a sudden change in index and, in keeping with Snell's law, should change its propagation direction. In fact, the output beam should bend toward the normal to the face, since it is traveling from a medium of low index ($n < 1$) to free space. This refractive effect is the opposite of that observed in a conventional dielectric, where the wave would travel from a high-index ($n > 1$) medium to free space, bending away from the normal.

A THz receiver is scanned along an arc to detect the output signals at various angular positions given by θ [Figure 3(a)]. The electric field amplitude spectra of the detected signals are shown in Figure 3(c) for $b = 1$ mm (corresponding to $f_c = 0.15$ THz). As θ increases, the spectral content shifts to lower frequencies,

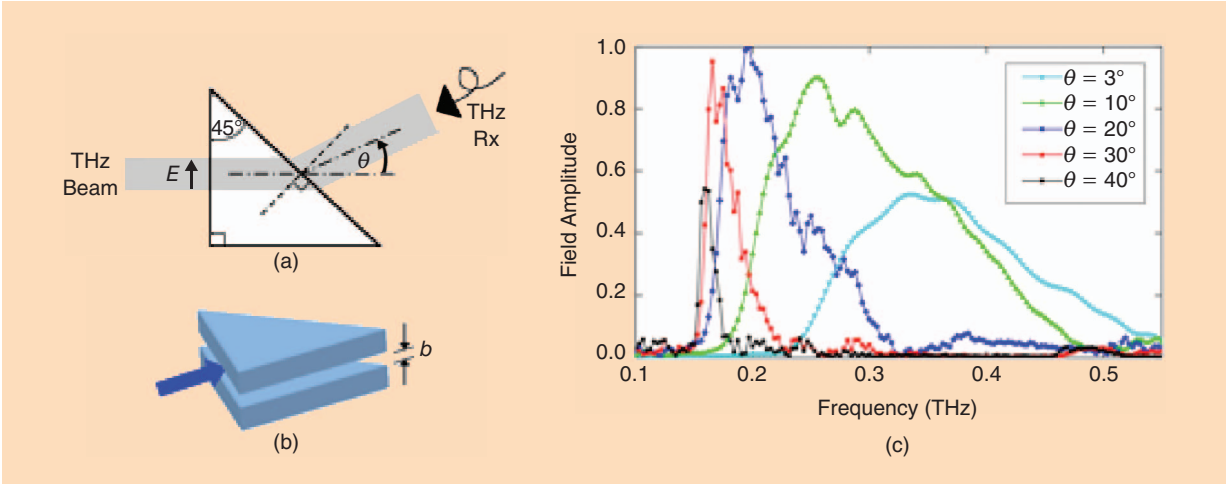

Figure 3. *(a) A schematic of the PPWG prism experiment. The width of the input face is 38.1 mm. (b) A 3-D rendition of the PPWG prism indicating the input beam. (c) Amplitude spectra of the detected signals at various receiver angular positions. Here, $b = 1$ mm and $f_c = 0.15$ THz. (From [6].)*

reaching frequencies near f_c at 45°. This demonstrates the frequency-dependent beam refraction at the angled output facet. Using these spectra, one can derive the values of the refractive indices experienced by the beam inside the waveguide as a function of frequency. These values can be compared with the theoretical values derived from (1). This comparison, displayed in Figure 2(b), shows very good agreement and demonstrates that the space between the plates (which is just air) indeed acts as if it has a dispersive refractive index less than unity.

Total Internal Reflection

Since a wave entering the PPWG and propagating via the TE_1 mode travels from a high-index medium (free space, $n = 1$) to a low-index medium ($n < 1$), one can expect to observe the equivalent to the fundamental optical phenomenon of total internal reflection (TIR) [12], which, in this case, is total *external* reflection. Based on Snell's law, the critical angle θ for total reflection (TR) at the input face is given by $\sin\theta = n$. Substituting into (1) and simplifying, we find $f_{TR} = f_c / \cos\theta$, where $0 \le \theta < 90^\circ$. This means that a wave with frequency f_{TR} entering the PPWG at angle θ undergoes TR and does not propagate into the waveguide. When $\theta = 0^\circ$ (normal incidence), $f_{TR} = f_c$, the self-consistent cutoff condition of the TE_1 mode. The physical interpretation of this result is that, as θ increases from normal incidence, the apparent cutoff shifts from f_c to higher frequencies. In other words, as θ increases, more and more frequencies reach the critical angle and are prohibited from entering the waveguide.

To test this experimentally [6], one can use the PPWG configuration shown in Figure 4(a) and detect the output signals while varying the incidence angle θ by rotating the waveguide with respect to the input beam. As in the earlier example, the input wave is a broadband THz signal. The detected field amplitude spectra shown in Figure 4(b) clearly indicate an upshifting of the apparent cutoff as θ increases, confirming the expected total-reflection behavior.

Brewster's Effect

Next, one can demonstrate the Brewster's effect, another well-known fundamental optical phenomenon that results in total transmission (or no reflection) for *p*-polarized light traveling from one medium to another at a specific angle [12]. The angle at which this occurs, the Brewster's angle, is given by $\theta_B = \tan^{-1}(n_2/n_1)$, where n_1 and n_2 are the refractive indices of the input and output media. For a TE_1-mode wave traveling inside the PPWG and meeting a (virtual) boundary into free space ($n_2 = 1$), the electric field polarization would be similar to *p*-polarized light, and one could expect to see the Brewster's effect. In this case, to achieve (for example) a $\theta_B = 60^\circ$, one would need $n_1 = 0.577$. Based on the refractive index

To demonstrate the refractive behavior of this artificial dielectric medium, one can perform an experiment using a 45° PPWG prism, fabricated using triangular aluminum plates.

curves given in Figure 2(b), for a plate separation of 1 mm, this should occur at a frequency of approximately 0.18 THz.

To test this [6], one can use the PPWG configuration shown in Figure 5(a). The PPWG prism is fabricated using two aluminum plates shaped into identical equilateral triangles. As shown, the THz beam enters the prism at the first air/PPWG interface at normal incidence, reflects off of the second air/PPWG interface at an angle of 60° (while part of the energy escapes to free space), and then leaves the prism at the third interface at normal incidence. The amplitude spectrum corresponding to the detected signal is shown in Figure 5(b) by the black dotted curve. The spectrum indicates a *null* around 0.18 THz, signifying a zero reflection coefficient at the second air/PPWG interface, consistent with the Brewster's condition. Figure 5(b) also shows the magnitude of the theoretical reflection coefficient

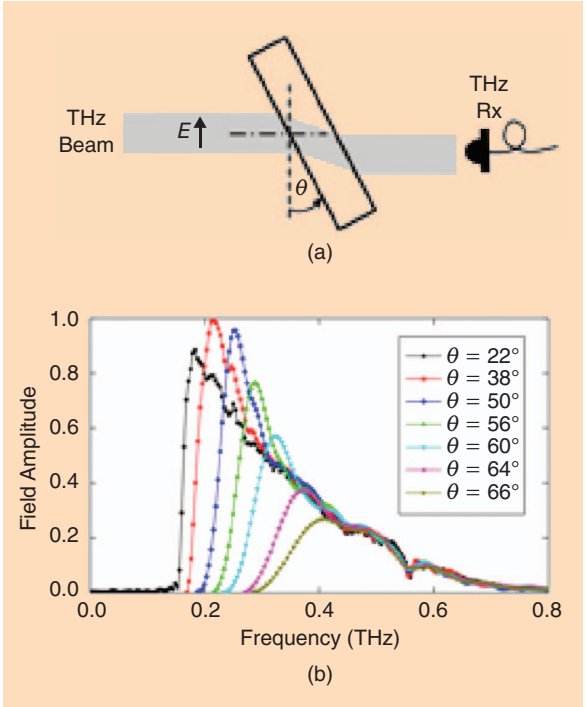

Figure 4. *(a) A schematic of the total-internal-reflection experiment. The width of the input face is 31.8 mm. (b) Amplitude spectra of the detected signals while rotating the PPWG with respect to the incident beam. Here, $b = 1$ mm and $f_c = 0.15$ THz. (From [6].)*

(red curve), computed for the second interface using the measured value of $b = 0.992$ mm and 60° incidence. The theoretical null is in excellent agreement with the experimental one at a frequency of 0.185 THz, confirming the Brewster's effect.

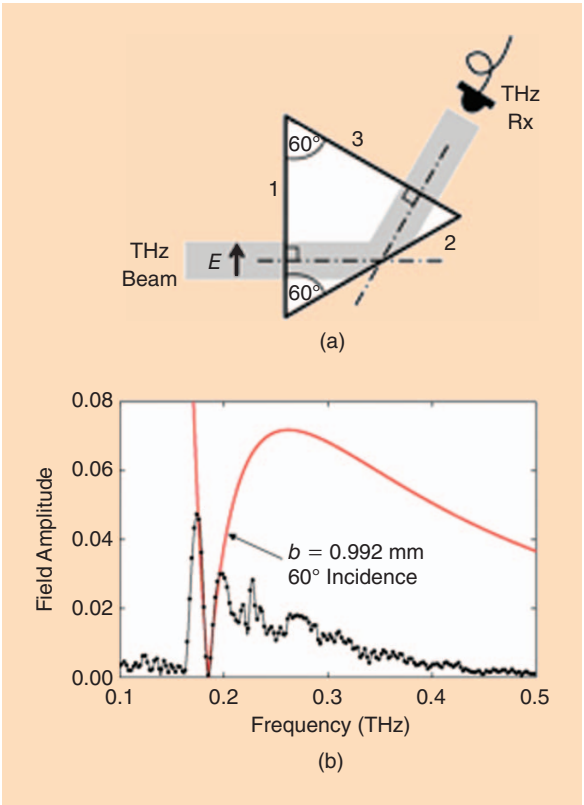

Figure 5. *(a) A schematic of the Brewster's-effect experiment. The width of the input face is 11.4 mm. (b) Amplitude spectrum of the signal reflected off of the second air/PPWG interface, compared to the theoretical reflection coefficient (red curve). Here, $f_c = 0.15$ THz. (From [6].)*

Lens with a One-Dimensional Focus

Using this artificial dielectric medium, one can also demonstrate a focusing lens [6]. Since the artificial dielectric medium has a refractive index less than that of free space, to achieve a focusing effect, one needs to use a concave geometry rather than the usual convex geometry employed with conventional dielectrics. The lens can be designed with a plano-concave geometry, as shown in Figure 6(a) and (b). As the THz beam propagates through the PPWG, it undergoes focusing only along one dimension, i.e., in the direction parallel to the plate surfaces, while the output beam diffracts in the perpendicular direction.

One can map the output beam profiles by scanning a slit aperture (oriented perpendicular to the plate surfaces) in a plane transverse to the optic axis. The beam profiles for representative frequencies of 0.16, 0.20, and 0.40 THz are shown in Figure 6(c) along with the theoretically computed Gaussian profile for 0.16 THz. These profiles demonstrate that the focusing effect of the lens gets stronger as the frequency decreases, which is opposite to a conventional dielectric lens that focuses higher frequencies more tightly. At a frequency of 0.16 THz, the 20-mm input beam has been focused to a size of approximately 4 mm, clearly demonstrating its focusing power. A drawback of this lens is its inability to focus along two dimensions, which is the reason a slit-shaped aperture must be employed to map the output beam profiles. This drawback motivates the idea of stacking multiple waveguides to form an array, as in Figure 1.

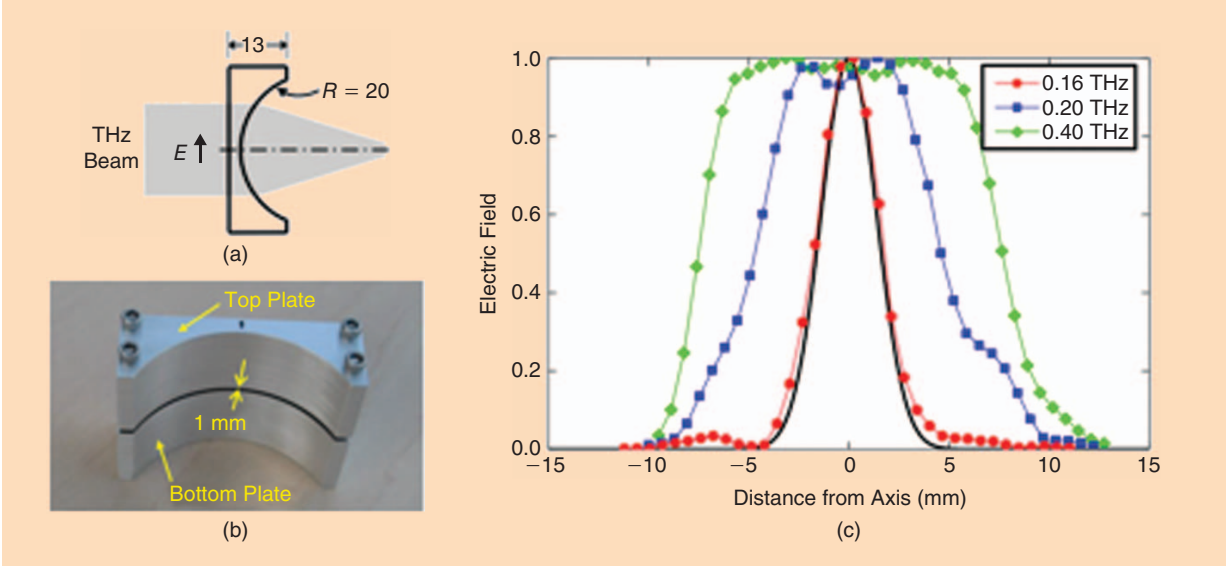

Figure 6. *(a) A schematic of the PPWG-lens experiment. The width of the input face is 40 mm. Dimensions are in millimeters. (b) A photograph of the fabricated device indicating the 1-mm gap between the plates. (c) Measured electric field profiles 35 mm away from the front surface. The solid black curve is the theoretical Gaussian profile for 0.16 THz. (From [6].)*

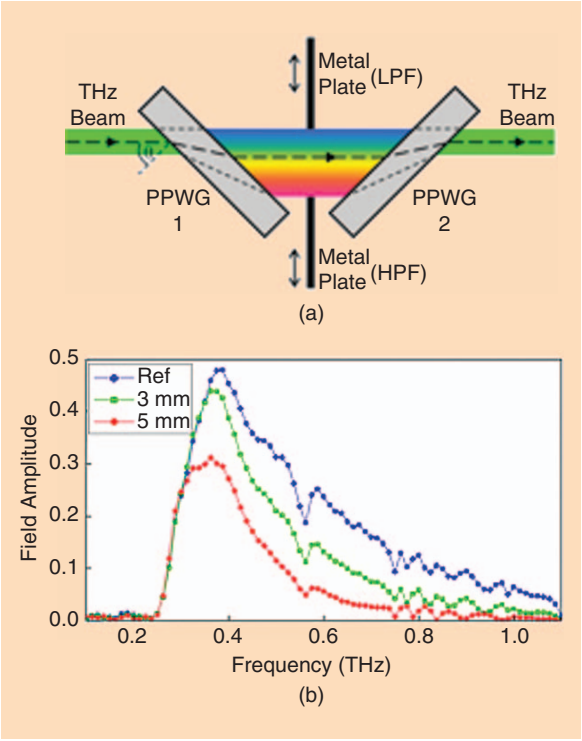

Figure 7. *(a) A schematic of the universal-filter experiment showing the two complementary PPWGs. The metal plates (beam blocks) used for the LPF and HPF are also shown. The spatial frequency spread is illustrated by the colors, where the high-frequency components are toward the blue side while the low-frequency components are toward the red side. (b) Amplitude spectra of the output signals for three different positions of the metal plate in the low-pass configuration. The reference (blue curve) is when the beam between the PPWGs is unblocked. Here, $b = 1$ mm and $f_c = 0.15$ THz. (Reproduced with permission from [7]. Copyright 2010, AIP Publishing LLC.)*

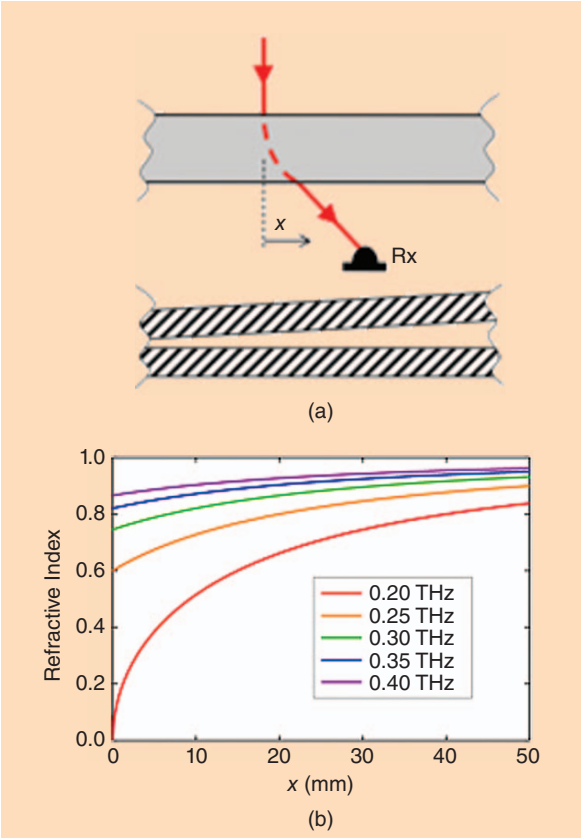

Figure 8. *(a) Plan view (top) of the experimental schematic and a cross-section (bottom) of the waveguide. The path of the THz beam is indicated by the (red) ray. The inclination of the top plate (0.72°) is exaggerated for clarity. Here, $b = 0.75$ mm when $x = 0$. (b) Calculated refractive index profiles, as a function of the transverse (x) coordinate, for several different frequencies. (Reproduced with permission from [8]. Copyright 2012, AIP Publishing LLC.)*

Tunable Universal Filter

One can also demonstrate a universal THz filter, capable of providing low-pass, high-pass, bandpass, and bandstop (or notch) filtering functionalities, along with continuous tunability of the cutoff frequencies [7]. In this case, the device geometry can consist of two complementary PPWGs as shown in Figure 7(a). The input THz beam is coupled into $PPWG_1$ at oblique incidence, polarized to excite the TE_1 mode. Because different frequency components experience different refractive indices inside the waveguide, Snell's law dictates that the direction of propagation inside the waveguide is frequency dependent. Since the refractive index varies monotonically from unity to zero as the frequency decreases, the beam exiting $PPWG_1$ is spatially chirped. This means that the high-frequency components lie closer to the input optic axis, while the low-frequency components are progressively displaced from the input optic axis. The spatially spread beam is then coupled into an identical $PPWG_2$, which is in a complementary geometry. This reverses the spatial chirp, combining the different frequency components back into a single output beam. This configuration is reminiscent of a four-prism dispersive delay line familiar in ultrafast optics and can be exploited in similar ways. For example, one can carry out various spectral filtering functions simply by blocking portions of the collimated but spatially chirped beam between the two waveguides.

Figure 7(b) illustrates the results of implementing a tunable low-pass filter (LPF). This is achieved simply by positioning a metal plate centrally between the two PPWGs and moving it perpendicularly into the path of the beam starting from the input optic axis (the high-frequency side). As the plate moves in, it blocks frequency components starting from the high-frequency end of the input spectrum, effectively realizing a LPF whose upper-cutoff frequency can be tuned by varying the position of the plate. Similarly, one can demonstrate a tunable high-pass filter by inserting a plate from the opposite side (the low-frequency side). One can also realize a bandpass and a bandstop filter by

The inhomogeneous artificial dielectric medium allows one to design and fabricate various GRIN optical devices that can provide unique functionality at THz frequencies.

positioning a metallic slit and a metallic strip, respectively, between the two PPWGs.

Bending THz Beams Using Inhomogeneous Artificial Dielectrics

As noted previously, it is also possible to realize an inhomogeneous medium in a PPWG, where the effective refractive index varies spatially, simply by adiabatically varying the plate separation. To validate this concept [8], one can use a simple geometry, starting from the conventional PPWG, by inclining one plate with respect to the other, such that the plate separation is varied along the dimension perpendicular to the propagation axis, as shown in Figure 8(a). In general, light rays propagating inside an inhomogeneous dielectric medium will bend toward the high-index region, an effect which is familiar in mirages and gradient-index (GRIN) lenses. Therefore, one could expect a THz beam propagating inside the waveguide to bend toward the region of larger plate separation.

The calculated refractive index profiles [using (1)] for this waveguide geometry at several frequencies are given in Figure 8(b). In this example, the inclination angle is 0.72°, and the plate separation at the input-axis position ($x = 0$) is 0.75 mm. These curves indicate that, for a given waveguide width, the index gradient decreases as the frequency increases. As in the case of a mirage, one can expect a larger index gradient to result in a higher degree of beam bending. This implies that the output beams corresponding to the low-frequency components would experience a greater deflection than the high-frequency components.

To extend this concept, one can demonstrate the bending of a THz beam around an object in its path—a true mirage effect [8]. The experimental geometry, a "roof" structure, is illustrated in Figure 9(a) and (b). Here, the top plate has two complementary flat inclined surfaces. The initial design can be carried out using a numerical ray-tracing program. Figure 9(b) gives the results for two rays corresponding to the frequencies of 0.16 and 0.54 THz, with the former being the design frequency. The (red) ray at the design frequency loops around the location of the hypothetical object, appearing to pass straight through the waveguide with minimal deviation. The (blue) ray at the other frequency passes through the location of the object and, therefore, would be affected by its presence. One can also perform full 3-D numerical simulations using the finite element method. This result is presented in Figure 9(c), which gives the electric field

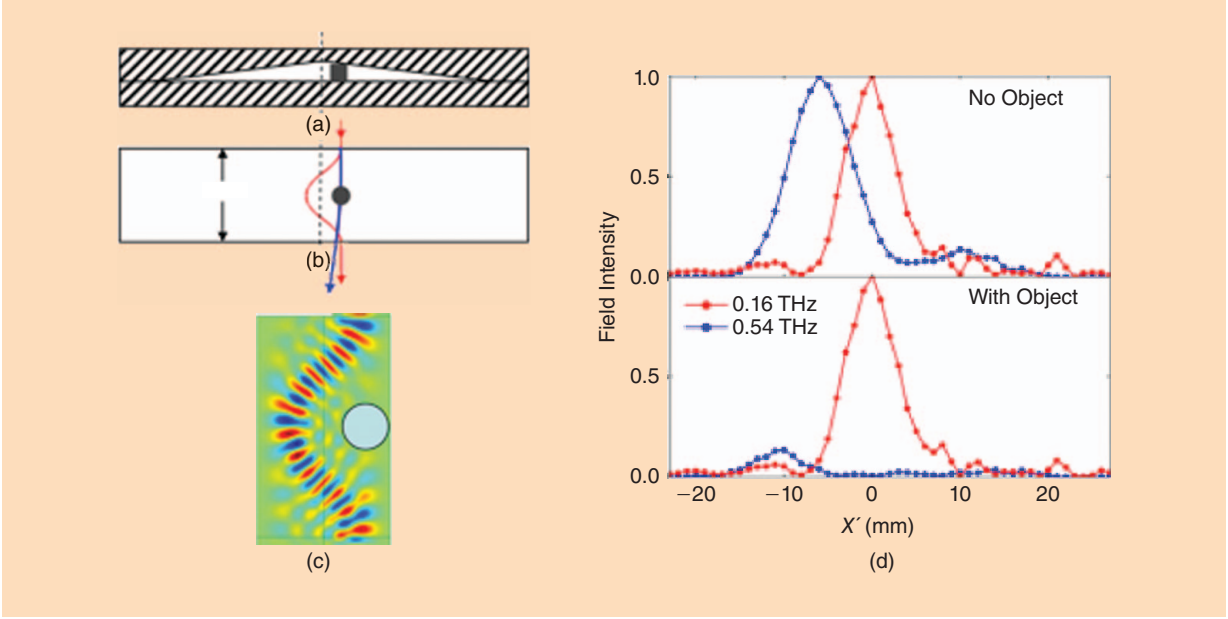

Figure 9. *(a) Cross-sectional view of the waveguide showing the "roof" shape of the guiding region with a cylindrical object placed inside. The inclination is exaggerated for clarity. (b) Plan view of the structure, showing the cylindrical object centered between the input and output faces. The red and blue curves are numerically computed ray paths corresponding to the frequencies of 0.16 THz and 0.54 THz, respectively. (c) Finite-element-method simulation of the beam path inside the waveguide corresponding to 0.16 THz. (d) A comparison of the experimentally measured output intensity profiles, corresponding to the same two frequencies, without (top) and with (bottom) the object inside the waveguide. (Reproduced with permission from [8]. Copyright 2012, AIP Publishing LLC.)*

(oriented parallel to the plate surfaces) distribution at the design frequency in a plane through the middle of the gap between the plates. Similar to the ray tracing, the curved path of the normally incident THz beam avoids the obstruction and emerges from the waveguide unaffected by its presence. At this frequency, the object [the circle in Figure 9(b) and (c)] is invisible to the THz beam.

For an experimental validation of these simulations, one can choose a waveguide with a length (along the input axis) of 5 cm, an inclination angle of 0.68°, and a solid metallic disc with a 10-mm diameter (corresponding to more than 5λ in size) as the object. After exciting the TE_1 mode at normal incidence using a 1-cm size THz beam, the output beam profiles can be mapped with and without the object in place at various frequencies. These intensity profiles are plotted in Figure 9(d) and show that the profile at the design frequency is virtually unaffected by the object inside the waveguide, whereas the one at the other frequency is significantly affected by the presence of the object. This proves that this waveguide geometry can be used to loop a THz beam around an object in its path, such that the beam does not see the object. This can be called an invisibility space, in contrast to an invisibility cloak, due to the limitations resulting from the requirement for the beam to enter the device at the proper position and input angle.

Maxwell's Fish-Eye Lens

The inhomogeneous artificial dielectric medium allows one to design and fabricate various GRIN optical devices that can provide unique functionality at THz frequencies. One type of exotic GRIN device is the Maxwell's fish-eye lens. This is a spherically symmetric lens that forms an image of each point on its surface to the diametrically opposite point on the surface, as shown in Figure 10(a). The refractive index distribution, as a function of the radial distance r from the lens center, is given by $n_o/[1+(r/R)^2]$, where R is the radius of the sphere and n_o is the maximum index. The index decrease from a value of n_o at the center to $n_o/2$ at the surface.

Using the two-plate waveguide structure, one can realize a cylindrically symmetric two-dimensional (2-D) version of this structure as shown in Figure 10(b) [9]. In this example, the top plate with an inner conical surface has been fabricated using 3-D printing and coated with silver paint to mimic a metallic surface. The bottom plate is a plain aluminum disk, which, together with the top plate, formed the necessary radially varying plate separation to achieve the index distribution for a Maxwell's fish-eye lens. As illustrated by the simulations in Figure 11(a) and (c), this lens is capable of imaging a 0.15-THz beam from a source located on its edge to the diametrically opposite location, regardless of the incidence angle.

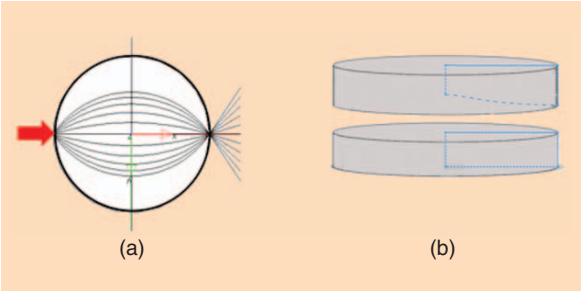

Figure 10. *(a) Ray-tracing simulation of the two-dimensional (2-D) Maxwell's fish-eye lens. (b) The 2-D Maxwell's fish eye lens, where the blue dotted curves indicate half of the cross-sectional profiles. (Reproduced with permission from [9]. Copyright 2013, AIP Publishing LLC.)*

Wave Plate

In the examples presented above, it is easy to imagine that all of the two-plate homogeneous artificial-dielectric structures can be generalized to the third dimension using a stacked multiplate geometry. This would of course increase the functionality of the devices and allow the manipulation of larger input beam sizes. Such a structure was recently demonstrated to create a wave-plate for the THz region [10]. As shown in Figure 12, the device consisted of a stacked array of metallic plates. In this case, unlike all previous examples, these plates contained many minute (subwavelength-sized) perforations.

When the electromagnetic wave is incident with a polarization parallel to the plates, it propagates via the TE_1 mode unhindered by the perforations, experiencing an index less than unity. However, when the wave is incident with a polarization perpendicular

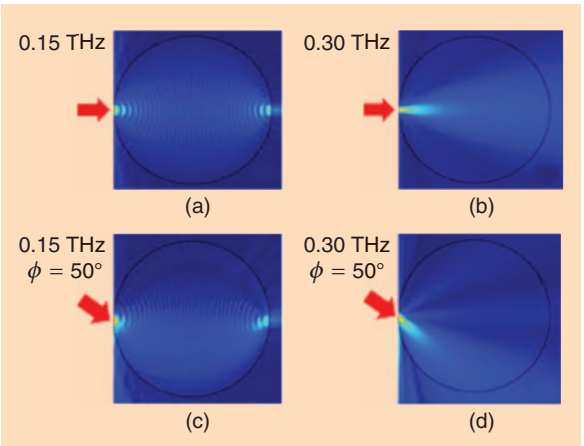

Figure 11. *Finite element method simulations of the electric field distribution at normal incidence for (a) 0.15 THz and (b) 0.3 THz and at 50° incidence for (c) 0.15 THz and (d) 0.5 THz. These indicate that the 0.15-THz (design frequency) beam is focused to the diametrically opposite point, regardless of the incidence angle. (Reproduced with permission from [9]. Copyright 2013, AIP Publishing LLC.)*

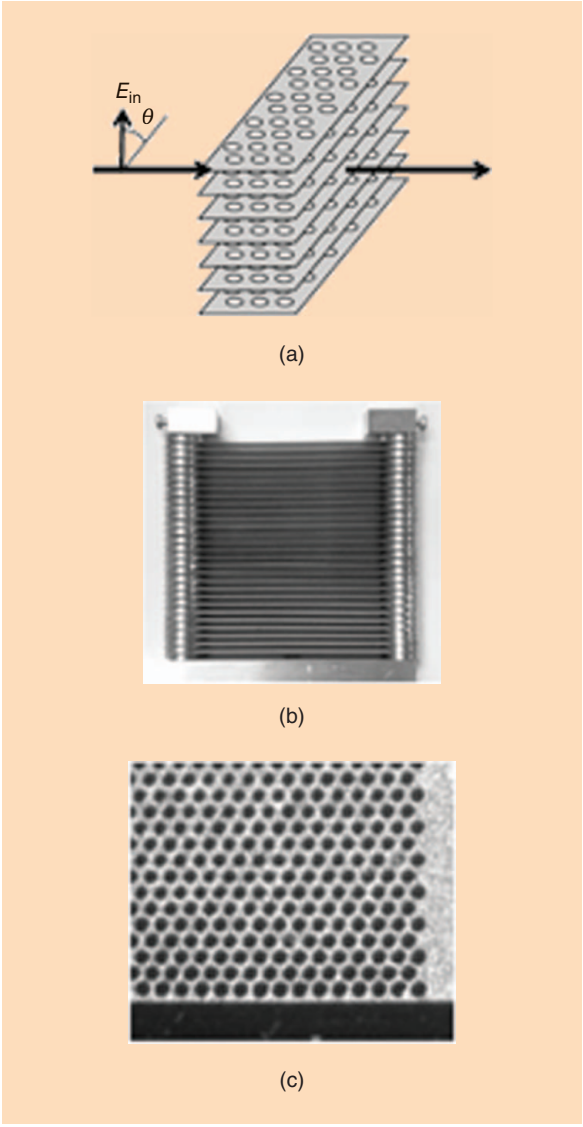

Figure 12. *(a) The structure of the wave-plate composed of stacked perforated metal plates. (b) A photograph of the device. (c) A close-up view of one of the perforated plates. (Reproduced with permission from [10].)*

to the plates, the perforations come into play, emulating a photonic-crystal effect. Consequently, the wave propagates via a transverse-magnetic (TM) mode experiencing a different refractive index. Since the two orthogonal polarizations encounter different indices, this structure behaves as a birefringent material. Therefore, by allowing part of the incident beam to travel via the TE mode and the rest to travel via the TM mode, one can achieve any given phase shift between the two orthogonal components. This is essentially a wave-plate that can modify the state of polarization of a THz beam [12].

Conclusion

We have presented a review of the design and applications of waveguide-based artificial dielectrics in the THz regime. This work clearly demonstrates the promise of this concept as a new paradigm for controlling and manipulating THz radiation. In addition to the applications mentioned, the homogeneous version of the medium can be used to realize a polarizing beam-splitter that can split a THz beam into two orthogonal polarization components. Furthermore, using the inhomogeneous version of the medium, other GRIN devices, such as the Luneburg lens and the Eaton lens, can be realized. In fact, this artificial medium will solve the long-standing problem of achieving high index gradients, which has hampered the practical realization of powerful GRIN devices using naturally conventional dielectric media.

A thorough investigation into the complete propagation behavior (attenuation and dispersion) of the TE_1 mode, including the input/output coupling efficiency, can be found in [13] and [14]. We hope this review will inspire more work in this exciting area, where ordinary metallic waveguides mimic dielectric media having extraordinary properties.

References

[1] R. E. Collin, *Field Theory of Guided Waves*. New York: IEEE Press, 1991.

[2] W. E. Kock, "Metal-lens antennas," *Proc. IRE*, vol. 34, no. 11 pp. 828–836, 1946.

[3] N. M. Rust, "The phase correction of horn radiators," *J. Inst. Electr. Eng.*, vol. 93, no. 1, pp. 50–51, 1946.

[4] O. M. Stuetzer, "Development of artificial microwave optics in Germany," *Proc. IRE*, vol. 38, no. 9, pp. 1053–1056, 1950.

[5] J. Brown, "Artificial dielectrics having refractive indices less than unity," *Proc. Inst. Elect. Eng.*, vol. 100, no. 5, pp. 51–62, 1953.

[6] R. Mendis and D. M. Mittleman, "A 2-D artificial dielectric with $0 \leqslant n < 1$ for the terahertz region," *IEEE Trans. Microwave Theory Tech.*, vol. 58, no. 7, pp. 1993–1998, 2010.

[7] R. Mendis, A. Nag, F. Chen, and D. M. Mittleman, "A tunable universal terahertz filter using artificial dielectrics based on parallel-plate waveguides," *Appl. Phys. Lett.*, vol. 97, no. 13, p. 131106, 2010.

[8] R. Mendis, J. Liu, and D. M. Mittleman, "Terahertz mirage: Deflecting terahertz beams in an inhomogeneous artificial dielectric based on a parallel-plate waveguide," *Appl. Phys. Lett.*, vol. 101, no. 11, pp. 111108–111108-4, 2012.

[9] J. Liu, R. Mendis, and D. M. Mittleman, "A Maxwell's fish eye lens for the terahertz region," *Appl. Phys. Lett.*, vol. 103, no. 3, p. 031104, 2013.

[10] M. Nagai, N. Mukai, Y. Minowa, M. Ashida, J. Takayanagi, and H. Ohtake, "Achromatic THz wave plate composed of stacked parallel metal plates," *Opt. Lett.*, vol. 39, no. 1, pp. 146–149, 2014.

[11] N. Marcuvitz, *Waveguide Handbook*. London, U.K.: Peregrinus, 1993.

[12] E. Hecht, *Optics*. San Francisco, CA: Addison-Wesley, 2002.

[13] R. Mendis and D. M. Mittleman, "An investigation of the lowest-order transverse-electric (TE_1) mode of the parallel-plate waveguide for THz pulse propagation," *J. Opt. Soc. Amer. B*, vol. 26, no. 9, pp. A6–A13, 2009.

[14] R. Mendis and D. M. Mittleman, "Comparison of the lowest-order transverse-electric (TE_1) and transverse-magnetic (TEM) modes of the parallel-plate waveguide for terahertz pulse applications," *Opt. Exp.*, vol. 17, no. 17, pp. 14839–14850, 2009.